HHS Public Access

Author manuscript

Integr Biol (Camb). Author manuscript; available in PMC 2015 October 06.

Published in final edited form as:

Integr Biol (Camb). 2015 October 5; 7(10): 1120–1134. doi:10.1039/c5ib00040h.

Human Breast Cancer Invasion and Aggression Correlates with ECM Stiffening and Immune Cell Infiltration

I Acerbi[1,*], **L Cassereau**[1,*], **I Dean**[1], **Q Shi**[2,6], **A Au**[3], **C Park**[4], **YY Chen**[5], **J Liphardt**[2,6], **ES Hwang**[7], and **VM Weaver**[1,2,8,9]

[1]Center for Bioengineering and Tissue Regeneration, Department of Surgery, UCSF, San Francisco, CA

[2]Bay Area Physical Sciences Oncology Center

[3]Department of Pathology, UCSF, San Francisco, California

[4]Department of Radiation Oncology, UCSF, San Francisco, CA

[5]Department of Pathology, UCSF, San Francisco, CA

[6]Department of Bioengineering, Stanford University, Palo Alto, CA

[7]Department of Surgery, Duke University Comprehensive Cancer Center, Durham, North Carolina, USA

[8]Departments of Anatomy and Bioengineering and Therapeutic Sciences, Eli and Edythe Broad Center of Regeneration Medicine and Stem Cell Research, and UCSF Helen Diller Comprehensive Cancer Center, UCSF, San Francisco, California, USA

Abstract

Tumors are stiff and data suggest that the extracellular matrix stiffening that correlates with experimental mammary malignancy drives tumor invasion and metastasis. Nevertheless, the relationship between tissue and extracellular matrix stiffness and human breast cancer progression and aggression remains unclear. We undertook a biophysical and biochemical assessment of stromal-epithelial interactions in noninvasive, invasive and normal adjacent human breast tissue and in breast cancers of increasingly aggressive subtype. Our analysis revealed that human breast cancer transformation is accompanied by an incremental increase in collagen deposition and a progressive linearization and thickening of interstitial collagen. The linearization of collagen was visualized as an overall increase in tissue birefringence and was most striking at the invasive front of the tumor where the stiffness of the stroma and cellular mechanosignaling were the highest. Amongst breast cancer subtypes we found that the stroma at the invasive region of the more aggressive Basal-like and Her2 tumor subtypes was the most heterogeneous and the stiffest when compared to the less aggressive Luminal A and B subtypes. Intriguingly, we quantified the greatest number of infiltrating macrophages and the highest level of TGF beta signaling within the cells at the invasive front. We also established that stroma stiffness and the level of cellular TGF

[9]Correspondence to: Valerie M. Weaver, Center for Bioengineering and Tissue Regeneration, Department of Surgery, University of California, San Francisco, 513 Parnassus Avenue, HSE-565, San Francisco, CA 94143, Valerie.Weaver@ucsf.edu, Telephone: (415) 476-3826, Fax: (415) 476-3985.

*Denotes equal contribution

beta signaling positively correlated with each other and with the number of infiltrating tumor-activated, macrophages, which was highest in the more aggressive tumor subtypes. These findings indicate that human breast cancer progression and aggression, collagen linearization and stromal stiffening are linked and implicate tissue inflammation and TGF beta.

Introduction

Human tumors are stiffer than normal tissue and this characteristic has been used to detect and stage cancer[1,2]. Experimental models indicate that altered tumor mechanics reflects increased interstitial pressure and compression loading, extracellular matrix (ECM) stiffening, and elevated cell contractility and rheology[3-6]. Mouse studies further suggest that the aberrant mechanics in cancerous tissue contributes to tumor aggression and compromises treatment efficacy[7-9]. These findings emphasize the need to characterize the origins of the altered tumor mechanics so that strategies to normalize tissue force can be identified for clinical use.

A major contributor to tumor mechanics is the abundant collagen-rich ECM which is a characteristic trait of many solid cancers[10-13]. This phenotype is particularly evident in human breast cancers which are characterized by a profound desmosplastic response that is accompanied by greater amounts of ECM and increased remodeling and cross-linking. We and others showed that the ECM progressively stiffens in mouse models of mammary cancer and that this stiffened ECM can foster tissue transformation and metastasis[6,9,14]. Consistently, unconfined compression analysis indicates that as human breast tissue transforms it progressively stiffens and suggests that tumor stiffness reflects a more aggressive cancer[15,16]. However, a recent study which employed micro indentation Atomic Force Microscopy (AFM) scanning analysis of invasive human breast and mouse mammary cancers underscored the heterogeneous stiffness of breast cancers and postulated that tumor aggression inversely correlates with tumor tissue stiffness[17]. Thus, the relevance of tumor mechanics and in particular ECM stiffness to human cancer progression and aggression remains unresolved.

In ductal carcinoma in situ (DCIS) the presence of linearized thick collagen fibers perpendicular to the tumor boundary associates with a higher propensity for progression to invasive breast cancer[18]. Collagen abundance in the primary breast tumor is also a significant risk factor for patient mortality[19]. Indeed, breast cancer patients with high levels of the collagen cross-linker lysyl oxidase (LOX) have a higher probability of developing metastatic lesions[14,20-23]. Because collagen stiffness increases as a function of concentration, fiber width and with LOX-mediated cross-linking these findings imply that ECM stiffness promotes malignancy and enhances tumor aggression in breast cancer patients[7]. Consistently, higher grade DCIS lesions, which have an elevated frequency of malignant transformation often have detectable levels of activated focal adhesion kinase (FAK) and p130Cas; two mechanically-activated kinases[24-27]. Moreover, breast cancer patients with abundant beta 1 integrin and activated FAK exhibit a poor overall prognosis[28,29]. Nevertheless, despite the fact that these findings argue that breast cancer progression and aggression are linked to ECM stiffening no study to date has systemically

connected collagen status, ECM mechanics and mechanosignaling to human breast cancer progression and tumor subtype. To address this deficiency we interrogated the status of ECM mechanics in human breast cancer as a function of histopathology and correlated these measurements with collagen architecture and tumor cell mechanosignaling with the objective of aligning these metrics to a specific biological phenotype.

We performed a comprehensive biophysical and histological analysis of human breast tissue to assess the biomechanical tissue characteristics relative to tumor progression and subtype. Human breast tumor biopsies with adjacent normal, DCIS and invasive breast cancer were examined to establish correlations between ECM and collagen architecture, ECM stiffness, epithelial mechanosignaling and tumor progression. Human breast biopsy tissues from normal mammary reduction mammoplasty and prophylactic mastectomy tissue with normal histological features were compared to stage matched, breast cancer samples from Luminal A, Luminal B, Her2 and Basal-like invasive breast cancers to establish associations with tumor subtype and aggression. The mechanical properties of the ECM, including ECM architecture and elasticity, were compared with indicators of pro-invasion tumor cell signaling and a tissue inflammatory response. Our data reveal, for the first time, that human breast cancer transformation is not only accompanied by a progressive deposition and remodeling of type I collagen and elevated tumor cell mechanosignaling, but that these phenotypes associate positively with a stiffened ECM that is the most rigid at the invasive front of the lesion. Moreover, amongst breast cancer subtypes we observed that the invasive front in the most aggressive subtypes (Basal-like, Her2) was the stiffest and most heterogeneous and contained cells with the highest mechanosignaling as compared to the less aggressive subtypes (Luminal A, Luminal B). Importantly, we quantified abundant infiltrating immune cells and the highest tissue levels of TGF beta signaling within the cells at the invasive front; regardless of subtype, and showed that both ECM stiffness and cellular TGF beta signaling correlated positively with the number of infiltrating macrophages of which many were activated. These findings demonstrate a positive association between breast tumor progression and aggression, collagen linearization and tissue mechanics and implicate inflammation and TGF beta signaling in this phenotype.

Results

Human luminal breast cancer progression is accompanied by collagen deposition and remodelling

We conducted a biophysical analysis of interstitial collagens as a function of breast transformation in archived, human breast tumor biopsies (n=20, luminal subtype, stage matched, BRCA mutation negative) containing invasive breast cancer, ductal carcinoma in situ (DCIS) and adjacent normal tissue. Regions with confirmed invasive luminal ductal carcinoma (IDC) breast cancer lesions, DCIS and adjacent normal tissue were identified on H&E stained sections (Figure 1; top panel). Quantification of the amount of interstitial collagen surrounding each region in serial sections by trichrome staining demonstrated that the stromal region bordering the DICS lesions contained significantly more collagen and that this increased further in the IDC lesions (Figure 1A; second panel; quantified in Figure 1B; top bar graph). Polarized imaging of picrosirius red stain parallel sections revealed that

these collagens were progressively assembled into thicker fibers (Figure 1A; third panel; quantified in Figure 1B; lower bar graph). Second harmonics generation (SHG) imaging using two-photon microscopy additionally revealed that the collagen fibers surrounding the DCIS lesions were more linearized, as compared to the collagens associated with the adjacent normal breast tissue, and that these linearized collagens appeared thicker in the stroma within the tissue regions contained the transformed IDC (Figure 1A; fourth panel). ImageJ (NIH[30]) and CT-Fire (LOCI, UW Madison) image processing software was used to render the collagen topography as imaris images and revealed that these linearized collagen fibers were significantly longer in the DCIS stroma and more uniform and oriented in the stroma surrounding the invasive lesions (Figure 1A; fifth panel; Figure 1C). These findings reveal a progressive increase in the content and a linear reorganization and orientation of interstitial collagen in human breast cancer as a function of malignant progression from normal through DCIS to a fully invasive IDC.

Human breast cancer progression is accompanied by elevated mechanosignaling and an increase in tissue birefringence

Quantitative polarization microscopy (Q-POL) is a method for quantifying the birefringence of a material such that it is insensitive to the orientation of the sample relative to the microscope[31,32]. The birefringence of a gel or a matrix is determined by fiber concentration and alignment. Once materials become aligned, such as when cells pull on a collagen-rich ECM, the birefringence increases. Thus, the highest birefringence in a tissue reflects a higher proportion of dense aligned "oriented" ECM bundles or fibers. Using Q-POL it is therefore possible to create a map of the retardance within a tissue section to reveal areas of ordered and/or concentrated fibrous material, especially ECM components such as collagen. Since Q-POL is a wide-field technique, it can be used to rapidly quantify collagen fiber concentration/alignment in relatively large samples with lateral dimensions of several millimetres[33]. Consistent with our PS and SHG analysis, Q-POL imaging revealed a progressive increase in birefringence within the human breast tissue between the normal adjacent and the DCIS regions that increased quite significantly in the region containing the invasive lesions; findings that reflecting an increased orientation of the interstitial, fibrillar collagens[34](Figure 2A; top panel; quantified in 2B; top bar graphs). Quantification of immunofluorescence images of the normal adjacent, DCIS and IDC tissue further revealed a progressive and significant increase in total levels of activated beta 1 integrin (activated β1 integrin), activated FAK (pY397 FAK) and higher cell contractility (pS19 MLC) within the epithelium; which reflect an increase in cellular mechanosignaling (Figure 2A; lower three panels; quantified in Figure 2B bar graphs)[9,35]. The elevated mechanosignaling in the cellular fraction associated with the oriented collagen fibers suggests that the interstitial ECM has a higher tensile strength that engages and activates cellular mechanotransduction.

The invasive front of human breast cancers is stiffer

We next assessed the relationship between collagen abundance and orientation and stromal stiffness in IDC specimens. Sections of snap frozen fresh human breast tissue containing luminal IDC lesions were fixed and stained by H&E and subjected to analysis by a pathologist to identify adjacent normal, the noninvasive region of the tumor and the invasive front of the tumor (Figure 3A; left image). Serial sections of the tissue were then stained

with propidium iodide to visualize the nuclei (Figure 3A; right image). Nanoscale atomic force microscopy (AFM) mechanical testing was then used to measure the elasticity of the stroma in 90x90μm^2 grids within these identified regions and to construct force maps of these indented areas[6] (Figure 3B,C). Q-POL imaging was then used to identify multiple sub regions within the stroma of the tissues lacking birefringence in the adjacent normal and within noninvasive regions surrounding the tumor as well as several additional regions with high birefringence within the IDC invasive front (Figure 3D; regions of interest are indicated by a dashed yellow box). We noted a strong association between intense Q-POL birefringence imaging measurements and stromal stiffness; particularly in the invasive leading edge of the IDC lesions where we quantified up to a 4 fold increase in the average elastic modulus relative to the non-invasive regions and the normal adjacent stroma (Figure 3C,D). Importantly, an examination of the distribution of stromal stiffness revealed a dramatic increase in stromal stiffness heterogeneity in the invasive region of the IDC tissue (Figure 3E). Thus, while the normal and noninvasive stroma and in the breast tissue of these cancer patients was predominantly around 400Pa; the invasive regions exhibited an elevated mean stiffness primarily due to a higher incidence of discrete, highly stiff regions (>5kPa). Additionally, we compared the biophysical properties of the tumor invasive front and tumor core (Figure 3F-I) and found that the tumor core tissue had less birefringence and was overall were less stiff. These findings link collagen orientation and linearization, tissue birefringence and elevated mechanosignaling to stromal stiffness. The data further emphasize the heterogeneity of the ECM and stromal stiffness in breast tumors and indicate that this phenotype is particularly evident at the invasive front of the lesion.

Human breast cancer progression associates with macrophage infiltration and elevated TGF beta signaling

Human breast cancers have high numbers of infiltrating immune cells and malignant progression in experimental models is associated with inflammation and metastasis can be inhibited by reducing macrophage recruitment[36-38]. Macrophages secrete a number of soluble factors including growth factors and metalloproteinases and transforming growth factor beta (TGF beta) that stimulate cell migration and induce ECM deposition, remodelling and cross-linking to stiffen the extracellular stroma[14,36,39]. Consistently, immunohistochemical staining of serial sections of the mechanically activated breast tumor biopsies shown in figures 1-3 revealed that they contained high numbers of CD45 positive immune cells (Figure 4A; top panel). Interestingly we noted that the CD45 positive immune cells were most abundant within the IDC region of the tissue and furthermore that they were particularly concentrated within the invasive front of these lesions where we also measured the most robust birefringence and the highest ECM stiffness (Figure 4A; top panel; Figure 3C). CD68 staining revealed that a high proportion of the infiltrating immune cells were macrophages which we confirmed were localized predominantly within the invasive regions of the IDC (Figure 4A; middle panel; quantified in bar graphs at left in B). CD163 staining confirmed these were indeed macrophages and indicated that they were activated[36]. Moreover, immunohistochemistry analysis indicated that the cells within the invasive front of the tumors had the highest TGF beta activity, as revealed by intense SMAD phosphorylation (Figure 4A; bottom panel; quantified in bar graphs at right in B)[40]. These data suggest there likely exist a functional relationship between tissue mechanics, infiltrating

"activated" macrophages and TGF beta signalling and malignant transformation of human breast cancers.

Tissue mechanics and collagen linearization associate with human breast cancer aggression

To determine if there is a relationship between tumor aggression and tissue mechanics we examined stage and size matched, untreated, human breast cancer biopsies representing four pathologically-confirmed subtypes classified as progressively aggressive including: least aggressive luminal A, luminal B, Her2+ and the most aggressive, basal-like triple negative (TNBC) (n=5 patients/subtype, stage matched, BRCA mutation negative)[41]. The invasive front of each lesion was identified in H&E stained tissue sections (Figure 5A; top panel). Polarized imaging of picrosirius red stained tissue revealed the most abundant fibrillar collagens were present at the invasive front of the Her2+ and TNBCs (Figure 5; second panel; quantified in top bar graphs shown in Figure 5B). SHG imaging revealed that these collagen fibers were more linearized and thicker in the more aggressive tumor subtypes (Figure 5A; third panel) a finding that was confirmed by the significant increase in tissue birefringence (Q-POL) quantified in the Her2+ and TNBCs (Figure 5A; bottom panel; quantified in lower bar graphs shown in Figure 5B). Moreover, AFM indentation indicated that the invasive front in the higher grant Her2+ and TNBCs were significantly stiffer than the less aggressive luminal breast tumors. Furthermore, analysis of immunofluorescence images of the invasive front of the luminal A, luminal B, Her2+ and TNBC biopsied tissue revealed that the cells within the more aggressive tumor subtypes (Her2+, TNBC) had the highest levels of activated β1 integrin (Activated β1 integrin) and FAK (^{pY397}FAK) and were more contractile (^{pS19}MLC) indicating they were likely more mechanically activated (Figure 6A; images quantified in bar graphs shown in B)[9,35]. Consistently, the higher grade tumor subtypes Her2+ and TNBC both showed much higher nuclear levels of the mechanically-activated factor Yorkie Associated Protein (YAP) than the lower grade luminal A/B tumors (Figure 6C; quantified in the bar graphs shown in Figure 6D)[42-44]. These findings confirm our earlier results which emphasize that there exists a positive correlation between stromal stiffness and the presence of linearized collagen fibers. The data also indicate that tissue mechanics and ECM modeling and collagen linearization reflect tumor aggression in human breast cancers.

Human breast cancer aggression correlates with a stiffer, more heterogeneous stroma and higher levels of infiltrating macrophages

Nanoscale AFM testing of the distribution and the magnitude of stromal stiffness at the invasive front of each breast tumor subtype revealed a striking increase in heterogeneity as a function of tumor aggressiveness. Thus, while AFM indentation revealed that acquisition of an invasive phenotype is consistently accompanied by a significant shift towards higher stiffness relative to prophylaxis tissue (Representative AFM indentation maps shown in Figure 7A), the distribution of the stromal stiffening was found to increase dramatically with tumor aggression (Figure 7B compare Luminal A to Luminal B to Her2+ to Basal-like [TNBC]). Thus, the two more aggressive breast tumor subtypes, Her2+ and TNBC had a much wider distribution of stiffness measurements and a greater skewing towards high values (>5kPa). Interestingly, IHC staining revealed that the skewed distribution towards

high ECM stiffness values found in the high aggressive cancer subtypes is mirrored by an increased number of infiltrating immune cells (CD45+ cells) and specifically macrophages (CD68+ cells Figure 7; confirmed by CD163 not shown) that were highly concentrated at the invasive front of each of the lesions (Figure 8A; first two panels; CD68+ve cell quantification shown in bar graphs shown at left in Figure 8B). Moreover, IHC for activated SMAD (pSMAD; a marker of TGF beta signaling in the cell[40]) revealed significantly elevated TGF beta signaling in the cells within the invasive front of the more aggressive subtype (Figure 8A; bottom panel; quantified below in Figure 8B right bar graphs). Indeed, we observed a significant correlation between the number of infiltrating macrophages and the stiffness of the invasive tumor stroma and between the number of infiltrating macrophages and the intensity of TGF beta signaling in the cells at the invasive front of these human breast tumors. These results show an association between tissue mechanics and inflammation and suggest they may cooperate to drive breast tumor aggression.

Discussion

Here, we demonstrate a correlation between the mechanical properties of the ECM, immune cell infiltrate, tumor grade, subtype and aggression in human breast cancer samples. Indeed, we found that the transition from non-malignant tissue to an invasive ductal carcinoma corresponds with significant collagen deposition, linearization and bundling which leads to a stiffening of the ECM. Subsequently, these mechanical alterations parallel enhanced activation of mechanically-sensitive signaling pathways associated with focal adhesions, YAP and growth factor receptor signaling. Accompanying this profound ECM remodeling and stiffening we quantified a significant immune cell infiltrate, predominantly comprised of "activated" pro-tumorigenic macrophages. We found that this influx of macrophages correlated with upregulated SMAD signaling in tumors, consistent with prior reports that infiltrating immune cells in tumors secrete abundant TGFβ to stimulate tumor and stromal TGFβ signaling. This presents a possible mechanistic explanation for the fibrosis and stiffening of the ECM via TGFβ-stimulated production of collagen and the collagen crosslinking enzyme lysyl oxidase (LOX)[45]. Interestingly, we also found that the relationship between ECM stiffness, immune infiltrate and tumor progression depended upon tumor subtype. Compared to Her2 and basal-like cancers, luminal breast cancers displayed less ECM remodeling and stiffening, and consistently less immune infiltrate and pro-invasion signaling. Further investigation into a causal relationship between ECM stiffening and the more aggressive breast cancer subtypes would present a new set of potential prognostic parameters.

Current clinical techniques interrogate tissue stiffness as a passive feature to detect cancer[46-48]. Yet, experimental models contend that tissue mechanics plays more than just a passenger role in tumor progression[9,35,49,50]. Amongst breast cancer subtypes, we found that the ECM at the invasive regions of the more aggressive Basal-like and Her2 tumor subtypes was the most heterogeneous and the stiffest when compared to the less aggressive Luminal A and B subtypes. While shear wave elastography (SWE) yields quantitative information capable of discerning benign and malignant lesions[51], our study demonstrates the need for region-specific measurements in deconstructing breast cancer mechanosignaling. The

topographical variations in the mechanical landscape of the collagen-rich ECM could not have detected by techniques such as SWE.

Interestingly, the mechanical heterogeneity within tumors observed in our study parallels the genomic intratumor heterogeneity observed in human cancers[52]. We found that geographically-distinct regions of the same tumor displayed different constituents, architectures and mechanical properties of the ECM. These results are consistent with previous publications demonstrating increased tumor stiffness relative to healthy tissue and further demonstrate the necessity for nanoscale mechanical testing and imaging to observe the heterogeneous structures and features contributing to tumor stiffness. Our findings, combined with evidence that multiple measures of heterogeneity are associated with poor patient prognosis, suggest the need for future exploration of how the resident stromal and immune environments influence tumor progression and fate. Correlating local mechanical measurements with regional histopathlogical analyses may provide the most efficacious approach to relating tumor behavior with ECM mechanics.

Experimental Methods

Human Breast Tissue—Fresh human breast tissue samples from prophylaxis mastectomy or breast tumor mastectomy were either embedded in OCT (Tissue-Tek) aqueous embedding compound within a disposable plastic base mold (Fisher) and were snap frozen by direct immersion into liquid nitrogen and kept at −80 degrees until cryosectioning for analysis, or formalin fixed and paraffin-embedded. All human breast tissue samples were prospectively collected from patients undergoing surgery at UCSF or Duke University Medical Center between 2010 and 2014. The selected samples were de-identified, stored and analyzed according to the procedures described in Institutional Review Board Protocol #10-03832 and #10-05046, approved by the UCSF Committee of Human Resources and the Duke IRB (Pro00034242).

Tissue preparation for AFM measurements of ECM stiffness

Human breast tissue samples were analyzed following cryopreservation. Frozen tissue blocks were then cut into 20 μm sections using disposable low profile microtome blades (Leica, 819) on a cryostat (Leica, CM1900-3-1). Prior to the AFM measurement, each section was fast thawed by immersion in PBS at thawed at room temperature. The samples were maintained in proteinase inhibitor in PBS (Protease Inhibitor Cocktail Roche Diagnostics, 11836170001), with Propidium Iodide (SIGMA P4170, 20 μg/ml) during the AFM session. Five patient's samples for each breast cancer subtype were used for AFM quantification of Young's elastic modulus of the cancer-associated stroma.

AFM measurements of ECM stiffness on tissue sections

All AFM indentations were performed using an MFP3D-BIO inverted optical AFM (Asylum Research) mounted on a Nikon TE2000-U inverted fluorescent microscope, as previously described [6]. Briefly, we used silicon nitride cantilevers with spring constant of 0.06 N/m with borosilicate glass spherical tip with 5 μm in diameter (Novascan Tech). The cantilever was calibrated using the thermal oscillation method prior to each experiment. Samples were indented at 20 μm/s loading rate, with a maximum force of 2 nN. Ten AFM

force maps were typically obtained on each sample, each map as a 50x50 μm raster series of indentations utilizing the FMAP function of the IGOR PRO build supplied by Asylum Research. The Hertz model was used to determine the elastic properties of the tissue (E1). Tissue samples were assumed to be incompressible and a Poisson's ratio of 0.5 was used in the calculation of the Young's elastic modulus.

Two-photon microscopy image acquisition and analysis

For two-photon imaging 20 μm fresh tissue sections were fixed post-AFM indentation in 4% neutral buffered formalin, and mounted with Permount Mounting Medium. We used custom resonant-scanning instruments based on published designs containing a five-PMT array (Hamamatsu, C7950) operating at video rate.[2] The setup was used with two channel Qultaneous video rate acquisition via two PMT detectors and an excitation laser (2W MaiTai Ti-Sapphire laser, 710-920nm excitation range). Second harmonics imaging was performed on a Prairie Technology Ultima System attached to an Olympus BX-51 fixed stage microscope equipped with a 25× (NA 1.05) water immersion objective. Tissue samples were exposed to polarized laser light at a wavelength of 830nm and emitted light was separated with a filter set (short pass filter, 720nm; dichroic mirror, 495nm; band pass filter, 475/40nm). Images of x-y planes of 284 by 284μm at a resolution of 0.656μm/pixel were captured using Micro-Manager Open Source Microscopy Software (Micro-Manager) in at least 3 locations on each human tissue sample. Quantification of collagen fibers was achieved by setting a minimal threshold in the second harmonic signal. The threshold was maintained for all images across all conditions. The area of regions that was covered by the minimal threshold was calculated and 3 images per sample were averaged together (Image J, Image Processing and Analysis in Java). Collagen fiber diameters data were visualized and analyzed using Imaris (Bitplane AG) and MATLAB (MathWorks). Statistical analysis was performed using Prism software (GraphPad Software, Inc.).

Q-POL image acquisition and analysis

Retardance maps of tissue samples were obtained using custom-written Matlab program to analyze the images acquired by an Olympus microscope (IX81) with a 10x objective as described previously (Qui et al., PNAS 2014). Briefly the light (632nm LED) is incident on the sample after passing through a linear top polarizer. After the sample, there is a circular polarizer consisting of a quarter waveplate and a linear polarizer with relative alignment angle of π/4. Rotation of the top polarizer (rotation angle θ) results in a sinusoidal modulation of the light intensity at each pixel[31,32]:

$$I(\theta) = \frac{I_0}{2}\left(1 + \sin\delta \cdot \sin(2\theta + 2\phi)\right) \quad (1)$$

where, ϕ is the principal axis and δ is the phase retardance (in radian) defined by

$$\delta = \frac{2\pi}{\lambda} \cdot \Delta n \cdot d. \quad (2)$$

The polarizer stage steps in 4° per step with a total of 200°. The light intensity modulation of each pixel on the image was fitted with equation 1 to generate the retardance map.

Picrosirius Red Staining and quantification—Flash frozen OCT embedded frozen tissues were crio-sectioned at 5 μm, fixed in 4% neutral buffered formalin and stained using 0.1% picrosirius red (Direct Red 80, Sigma) and counterstained with Weigert's hematoxilin, as previously described [34]. Polarized light images were acquired using an Olympus IX81 microscope fitted with an analyzer (U-ANT) and polarizer (U-POT, Olympus) oriented parallel and orthogonal to each other. Images were quantified using ImageJ. Briefly, a minimal intensity threshold was used to eliminate background and then fiber density was measured as image % area coverage. For analysis of tumor progression samples 5 images per tissue region (normal, DCIS, IDC) were taken for all 20 patients. Results per tissue region type were then pooled and averaged and normalized to adjacent normal tissue values. For analysis of breast cancer subtypes, 10 images were taken per patient with 5 patients per subtype. Results for each subtype were pooled and averaged and then normalized to data from prophylaxis tissue serving as a non-tumor control.

Trichrome Staining and quantification—Paraffin-embedded samples were sectioned at 5 μm and Masson's trichrome staining was performed following the optimized protocol (https://www.bcm.edu/research/labs/jeffrey-rosen/protocols). For quantitative morphometric analysis, ten sections of trichrome slides were imaged with color camera, using an Olympus IX81 microscope and bright field light. Three fields acquired in each of the histological regions of defined by our pathologist (Dr. YY Chen). Each RGB image was subsequently analyzed using Image J (version 1.32j) software (National Institutes of Health, USA http://rsb.info.nih.gov/ij/). The amount of fibrosis was then estimated from the RGB images with a macro written by the authors (IA) by converting pixels of the image with substantially greater (> 1.5) blue than red intensity ratio, and calculating the area over the threshold (Supplemental Figure I).

Immunohistochemistry staining and quantification

Antibodies and Reagents—Antibodies were as follows: CD45 (antibody clone X16/99 from Leica) CD68(antibody clone 514H12 from Leica), YAP (Rabbit Cell Signaling), pSMAD (Rabbit Cell Signaling). Immunohistochemistry staining and imaging of FFPE tissue sections was performed as recently described.

Quantification—pSMAD intensity was quantified as the integrated density divided by the total number of positive pSMAD-stained cancer cells. The integrated density was measured using ImageJ software (NIH). The integrated density was divided by the total number of positive pSMAD-stained cancer cells. Average YAP+ cells were quantified by the number of nuclear-stained YAP+ cancer cells divided the total number of cancer cells. The ratio of positive nuclear-stained YAP cells divided by the total number of cells was multiplied by 100 to generate a percentage.

Immunofluorescence Staining and quantification

Antibodies and Reagents—Antibodies were as follows: activated β1 integrin (Rat R&D Systems); FAKpY397 (Rabbit Invitrogen); Phospho Akt Substrate (Rabbit Cell Signaling); MLCpS19 (Rabbit Cell Signaling) secondary AlexaFluor goat anti-mouse, anti-rabbit, and anti-rat (488 conjugates) and DAPI (Sigma). Immunofluorescence staining and imaging of FFPE tissue sections was performed as recently described.

Quantification—Images were quantified in ImageJ. Briefly a minimal intensity threshold for real signal based on the max intensity of secondary only controls was used and then signal intensity per cell was quantified as image fluorescent intensity integrated density divided by the total number of cells in the image. For analysis of tumor progression samples 5 images per tissue region (normal, DCIS, IDC) were taken for all 20 patients. Results per tissue region type were then pooled and averaged and normalized to adjacent normal tissue values. For analysis of breast cancer subtypes, 10 images were taken per patient with 5 patients per subtype. Results for each subtype were pooled and averaged and then normalized to data from prophylaxis tissue serving as a non-tumor control.

Statistics

Statistical significance comparing different histological regions representing tumor progression within the same patient was assessed either using a two-tailed paired Mann-Whitney non-parametric test or ANOVA. Statistical significance comparing tissue samples from different tumor subtypes was assessed either using a two-tailed unpaired Mann-Whitney non-parametric test, Wilcoxon Rank Sum Test, or ANOVA as appropriate. Means are presented ± standard deviation of multiple measurements and statistical significance was considered at $P < 0.05$.

Supplementary Material

Refer to Web version on PubMed Central for supplementary material.

Acknowledgements

We thank the Dr. Janna Mouw and Dr. Michael Pickup as well as all members of the Weaver lab for helpful discussions and the tissue pathology cores at UCSF for assistance with tissue sectioning and staining. This work was supported by Susan G. Komen Postdoctoral Fellowship PDF12230246 (I.A.), US National Institutes of Health grant NCI F31 CA183255 (L.C.), ARCS Foundation Fellowship (L.C.), US National Institutes of Health grant T32 CA108462-11 (I.D.), US Department of Defense Breast Cancer Research Program (DOD BCRP) grant W81XWH-05-1-0330 and W81XWH-13-1-0216 (V.M.W.), US National Institutes of Health (NIH) NCI grants R01 CA192914-01 and U01 ES019458 (V.M.W.), NIH NCI grant U54 CA143836 (V.M.W. and J.L.), NIH NCI grant R01 CA174929 (V.M.W. and C.P.) and Susan G. Komen grant KG110560PP (V.M.W. and E.S.H.).

Works Cited

[1]. Youk JH, Son EJ, Gweon HM, Kim H, Park YJ, Kim J-A. Comparison of strain and shear wave elastography for the differentiation of benign from malignant breast lesions, combined with B-mode ultrasonography: qualitative and quantitative assessments. Ultrasound Med Biol. 2014; 40(10):2336–44. [PubMed: 25130444]

[2]. Chang JM, Moon WK, Cho N, Yi A, Koo HR, Han W, Noh D-Y, Moon H-G, Kim SJ. Clinical application of shear wave elastography (SWE) in the diagnosis of benign and malignant breast diseases. Breast Cancer Res Treat. 2011; 129(1):89–97.

[3]. Provenzano PP, Cuevas C, Chang AE, Goel VK, Von Hoff DD, Hingorani SR. Enzymatic targeting of the stroma ablates physical barriers to treatment of pancreatic ductal adenocarcinoma. Cancer Cell. 2012; 21(3):418–29. [PubMed: 22439937]

[4]. Tse JM, Cheng G, Tyrrell JA, Wilcox-Adelman SA, Boucher Y, Jain RK, Munn LL. Mechanical compression drives cancer cells toward invasive phenotype. Proc Natl Acad Sci U S A. 2012; 109(3):911–6. [PubMed: 22203958]

[5]. Samuel MS, Lopez JI, McGhee EJ, Croft DR, Strachan D, Timpson P, Munro J, Schröder E, Zhou J, Brunton VG, Barker N, Clevers H, Sansom OJ, I. Anderson K, Weaver VM, Olson MF. Actomyosin-mediated cellular tension drives increased tissue stiffness and β-catenin activation to induce epidermal hyperplasia and tumor growth. Cancer Cell. 2011; 19(6):776–91.

[6]. Lopez JI, Kang I, You W-K, McDonald DM, Weaver VM. In situ force mapping of mammary gland transformation. Integr Biol (Camb). 2011; 3(9):910–21. [PubMed: 21842067]

[7]. Dvorak HF, Weaver VM, Tlsty TD, Bergers G. Tumor microenvironment and progression. J Surg Oncol. 2011; 103(6):468–74.

[8]. Takai, P. Lu, K.; Weaver, VM.; Werb, Z. Extracellular matrix degradation and remodeling in development and disease. Cold Spring Harb Perspect Biol. 2011; 3(12)

[9]. Levental KR, Yu H, Kass L, Lakins JN, Egeblad M, T. Erler J, Fong SFT, Csiszar K, Giaccia A, Weninger W, Yamauchi M, Gasser DL, Weaver VM. Matrix crosslinking forces tumor progression by enhancing integrin signaling. Cell. 2009; 139(5):891–906.

[10]. Werb Z, Sympson CJ, Alexander CM, Thomasset N, Lund LR, MacAuley A, Ashkenas J, Bissell MJ. Extracellular matrix remodeling and the regulation of epithelial-stromal interactions during differentiation and involution. Kidney Int Suppl. 1996; 54:S68–74. [PubMed: 8731199]

[11]. Keely PJ. Mechanisms by which the extracellular matrix and integrin signaling act to regulate the switch between tumor suppression and tumor promotion. J Mammary Gland Biol Neoplasia. 2011; 16(3):205–19.

[12]. Hasebe T. Tumor-stromal interactions in breast tumor progression--significance of histological heterogeneity of tumor-stromal fibroblasts. Expert Opin Ther Targets. 2013; 17(4):449–60. [PubMed: 23297753]

[13]. Rudnick JA, Kuperwasser C. Stromal biomarkers in breast cancer development and progression. Clin Exp Metastasis. 2012; 29(7):663–72. [PubMed: 22684404]

[14]. Pickup MW, Laklai H, Acerbi I, Owens P, Gorska AE, Chytil A, Aakre M, Weaver VM, Moses HL. Stromally derived lysyl oxidase promotes metastasis of transforming growth factor-β-deficient mouse mammary carcinomas. Cancer Res. 2013; 73(17):5336–46. [PubMed: 23856251]

[15]. Samani A, Bishop J, Luginbuhl C, Plewes DB. Measuring the elastic modulus of ex vivo small tissue samples. Phys Med Biol. 2003; 48(14):2183–98. [PubMed: 12894978]

[16]. Samani A, Zubovits J, Plewes D. Elastic moduli of normal and pathological human breast tissues: an inversion-technique-based investigation of 169 samples. Phys Med Biol. 2007; 52(6):1565–76. [PubMed: 17327649]

[17]. Plodinec M, Loparic M, Monnier CA, Obermann EC, Zanetti-Dallenbach R, Oertle P, Hyotyla JT, Aebi U, Bentires-Alj M, Lim RYH, -A. Schoenenberger C. The nanomechanical signature of breast cancer. Nat Nanotechnol. 2012; 7(11):757–65. [PubMed: 23085644]

[18]. Conklin MW, Eickhoff JC, Riching KM, Pehlke CA, Eliceiri KW, Provenzano PP, Friedl A, J. Keely P. Aligned collagen is a prognostic signature for survival in human breast carcinoma. Am J Pathol. 2011; 178(3):1221–32. [PubMed: 21356373]

[19]. Hasebe T, Tsuda H, Tsubono Y, Imoto S, Mukai K. Fibrotic focus in invasive ductal carcinoma of the breast: a histopathological prognostic parameter for tumor recurrence and tumor death within three years after the initial operation. Jpn J Cancer Res. 1997; 88(6):590–9. [PubMed: 9263537]

[20]. Erler JT, Weaver VM. Three-dimensional context regulation of metastasis. Clin Exp Metastasis. 2009; 26(1):35–49.

[21]. Erler JT, Giaccia AJ. Lysyl oxidase mediates hypoxic control of metastasis. Cancer Res. 2006; 66(21):10238–41. [PubMed: 17079439]

[22]. Decitre M, Gleyzal C, Raccurt M, Peyrol S, Aubert-Foucher E, Csiszar K, Sommer P. Lysyl oxidase-like protein localizes to sites of de novo fibrinogenesis in fibrosis and in the early

stromal reaction of ductal breast carcinomas. Lab Invest. 1998; 78(2):143–51. [PubMed: 9484712]

[23]. L. Semenza G. Cancer-stromal cell interactions mediated by hypoxia-inducible factors promote angiogenesis, lymphangiogenesis, and metastasis. Oncogene. 2013; 32(35):4057–63.

[24]. van der Flier S, Brinkman A, Look MP, Kok EM, Meijer-van Gelder ME, Klijn JG, Dorssers LC, Foekens JA. Bcar1/p130Cas protein and primary breast cancer: prognosis and response to tamoxifen treatment. J Natl Cancer Inst. 2000; 92(2):120–7.

[25]. Tornillo G, Bisaro B, Camacho-Leal MDP, Galié M, Provero P, Di Stefano P, Turco E, Defilippi P, Cabodi S. p130Cas promotes invasiveness of three-dimensional ErbB2-transformed mammary acinar structures by enhanced activation of mTOR/p70S6K and Rac1. Eur J Cell Biol. 2011; 90(2-3):237–48. [PubMed: 20961652]

[26]. Oktay MH, Oktay K, Hamele-Bena D, Buyuk A, G. Koss L. Focal adhesion kinase as a marker of malignant phenotype in breast and cervical carcinomas. Hum Pathol. 2003; 34(3):240–5.

[27]. D. Planas-Silva M, D. Bruggeman R, Grenko RT, Stanley Smith J. Role of c-Src and focal adhesion kinase in progression and metastasis of estrogen receptor-positive breast cancer. Biochem Biophys Res Commun. 2006; 341(1):73–81. [PubMed: 16412380]

[28]. Barkan D, Chambers AF. β1-integrin: a potential therapeutic target in the battle against cancer recurrence. Clin Cancer Res. 2011; 17(23):7219–23. [PubMed: 21900388]

[29]. Cordes N, Park CC. beta1 integrin as a molecular therapeutic target. Int J Radiat Biol. 2007; 83(11-12):753–60. [PubMed: 18058364]

[30]. Schneider CA, Rasband WS, Eliceiri KW. NIH Image to ImageJ: 25 years of image analysis. Nature Methods. 2012; 9(7):671–675. [PubMed: 22930834]

[31]. Shin IH, Shin SM, Kim DY. New, simple theory-based, accurate polarization microscope for birefringence imaging of biological cells. J Biomed Opt. 2010; 15(1):016028. [PubMed: 20210472]

[32]. Glazer AM, Lewis JG, Kaminsky W. An Automatic Optical Imaging System for Birefringent Media. Proceedings of the Royal Society of London A: Mathematical, Physical and Engineering Sciences. 1996; 452(1955):2751–2765.

[33]. Shi Q, Ghosh RP, Engelke H, Rycroft CH, Cassereau L, Sethian JA, Weaver VM, Liphardt JT. Rapid disorganization of mechanically interacting systems of mammary acini. Proc Natl Acad Sci U S A. 2014; 111(2):658–63. [PubMed: 24379367]

[34]. Király K, Hyttinen MM, Lapveteläinen T, Elo M, Kiviranta I, Dobai J, Módis L, Helminen HJ, Arokoski JP. Specimen preparation and quantification of collagen birefringence in unstained sections of articular cartilage using image analysis and polarizing light microscopy. Histochem J. 1997; 29(4):317–27.

[35]. Paszek MJ, Zahir N, Johnson KR, Lakins JN, Rozenberg GI, Gefen A, Reinhart-King CA, Margulies SS, Dembo M, Boettiger D, Hammer DA, Weaver VM. Tensional homeostasis and the malignant phenotype. Cancer Cell. 2005; 8(3):241–54. [PubMed: 16169468]

[36]. Ruffell B, Au A, Rugo HS, Esserman LJ, S. Hwang and L. M. Coussens E. Leukocyte composition of human breast cancer. Proc Natl Acad Sci U S A. 2012; 109(8):2796–801. [PubMed: 21825174]

[37]. Ruffell B, Chang-Strachan D, Chan V, Rosenbusch A, Ho CMT, Pryer N, Daniel D, Hwang ES, Rugo HS, Coussens LM. Macrophage IL-10 blocks CD8+ T cell-dependent responses to chemotherapy by suppressing IL-12 expression in intratumoral dendritic cells. Cancer Cell. 2014; 26(5):623–37. [PubMed: 25446896]

[38]. Pollard JW. Macrophages define the invasive microenvironment in breast cancer. J Leukoc Biol. 2008; 84(3):623–30. [PubMed: 18467655]

[39]. Pickup M, Novitskiy S, Moses HL. The roles of TGFβ in the tumour microenvironment. Nat Rev Cancer. 2013; 13(11):788–99. [PubMed: 24132110]

[40]. Engel ME, Datta PK, Moses HL. Signal transduction by transforming growth factor-beta: a cooperative paradigm with extensive negative regulation. J Cell Biochem Suppl. 1998; 30-31:111–22. [PubMed: 9893262]

[41]. Goldhirsch A, Wood WC, Coates AS, Gelber RD, Thürlimann B, Senn HJ, Panel members. Strategies for subtypes--dealing with the diversity of breast cancer: highlights of the St. Gallen

International Expert Consensus on the Primary Therapy of Early Breast Cancer 2011. Ann Oncol. 2011; 22(8):1736–47. England. [PubMed: 21709140]

[42]. Janmey PA, Wells RG, Assoian RK, McCulloch CA. From tissue mechanics to transcription factors. Differentiation. 2013; 86(3):112–20.

[43]. H. Wrighton K. Mechanotransduction: YAP and TAZ feel the force. Nat Rev Mol Cell Biol. 2011; 12(7):404.

[44]. Low BC, Pan CQ, Shivashankar GV, Bershadsky A, Sudol M, Sheetz M. YAP/TAZ as mechanosensors and mechanotransducers in regulating organ size and tumor growth. FEBS Lett. 2014; 588(16):2663–70.

[45]. Lijnen P, Petrov V. Transforming growth factor-beta 1-induced collagen production in cultures of cardiac fibroblasts is the result of the appearance of myofibroblasts. Methods Find Exp Clin Pharmacol. 2002; 24(6):333–44. [PubMed: 12224439]

[46]. Fasching PA, Heusinger K, Loehberg CR, Wenkel E, Lux MP, Schrauder M, Koscheck T, Bautz W, Schulz-Wendtland R, Beckmann MW, Bani MR. Influence of mammographic density on the diagnostic accuracy of tumor size assessment and association with breast cancer tumor characteristics. Eur J Radiol. 2006; 60(3):398–404. [PubMed: 17030108]

[47]. Chang JM, Park IA, Lee SH, Kim WH, Bae MS, Koo HR, Yi A, Kim SJ, Cho N, Moon WK. Stiffness of tumours measured by shear-wave elastography correlated with subtypes of breast cancer. Eur Radiol. 2013; 23(9):2450–8. [PubMed: 23673574]

[48]. Evans A, Whelehan P, Thomson K, McLean D, Brauer K, Purdie C, Jordan L, Baker L, Thompson A. Quantitative shear wave ultrasound elastography: initial experience in solid breast masses. Breast Cancer Res. 2010; 12(6):R104. [PubMed: 21122101]

[49]. Mouw JK, Yui Y, Damiano L, Bainer RO, Lakins JN, Acerbi I, Ou G, Wijekoon AC, Levental KR, Gilbert PM, Hwang ES, Chen Y-Y, Weaver VM. Tissue mechanics modulate microRNA-dependent PTEN expression to regulate malignant progression. Nat Med. 2014; 20(4):360–7. [PubMed: 24633304]

[50]. Provenzano PP, Inman DR, Eliceiri KW, Keely PJ. Matrix density-induced mechanoregulation of breast cell phenotype, signaling and gene expression through a FAK-ERK linkage. Oncogene. 2009; 28(49):4326–43. [PubMed: 19826415]

[51]. Balleyguier C, Canale S, Ben Hassen W, Vielh P, Bayou EH, Mathieu MC, Uzan C, Bourgier C, Dromain C. Breast elasticity: principles, technique, results: an update and overview of commercially available software. Eur J Radiol. 2013; 82(3):427–34. [PubMed: 22445593]

[52]. McGranahan N, Swanton C. Biological and Therapeutic Impact of Intratumor Heterogeneity in Cancer Evolution. Cancer Cell. 2015; 27(1):15–26.

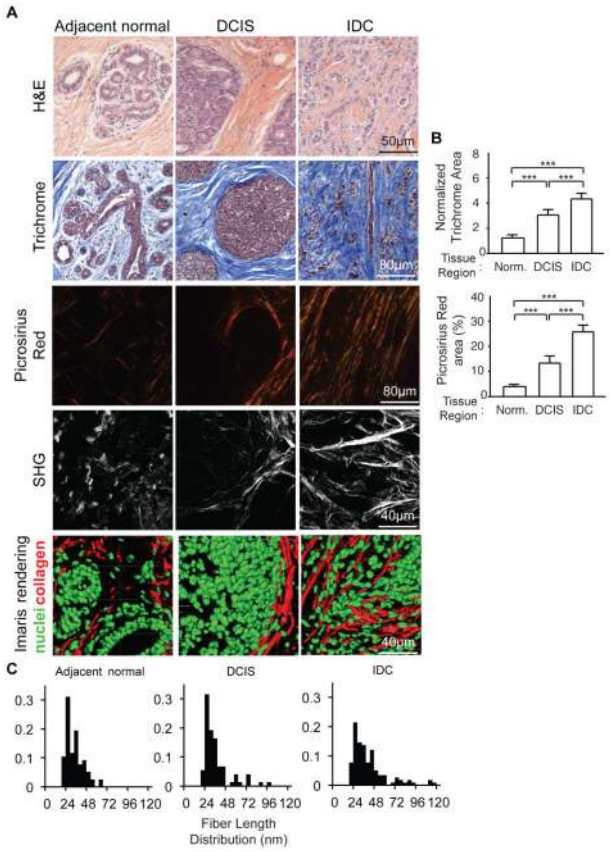

Figure 1. Tumor progression correlates with significant ECM remodeling

(A) Immunohistological staining (H&E, trichrome, picrosirius red, and second harmonic generation) and imaging of human tumor samples featuring areas of normal, DCIS and invasive ductal carcinoma (IDC). (B) Quantitative analysis of trichrome and picrosirus red staining as a measure of collagen density. Bars represent the average of 20 patient samples and error bars represent standard deviation. (*** denotes $P<0.05$) (C) Quantitative analysis of collagen fiber length from second harmonic generation imaging represented as a histogram. Statistical significance was determined via a Wilcoxon Rank Sum Test, with DCIS and IDC showing statistically significant differences relative to normal ($P<0.05$).

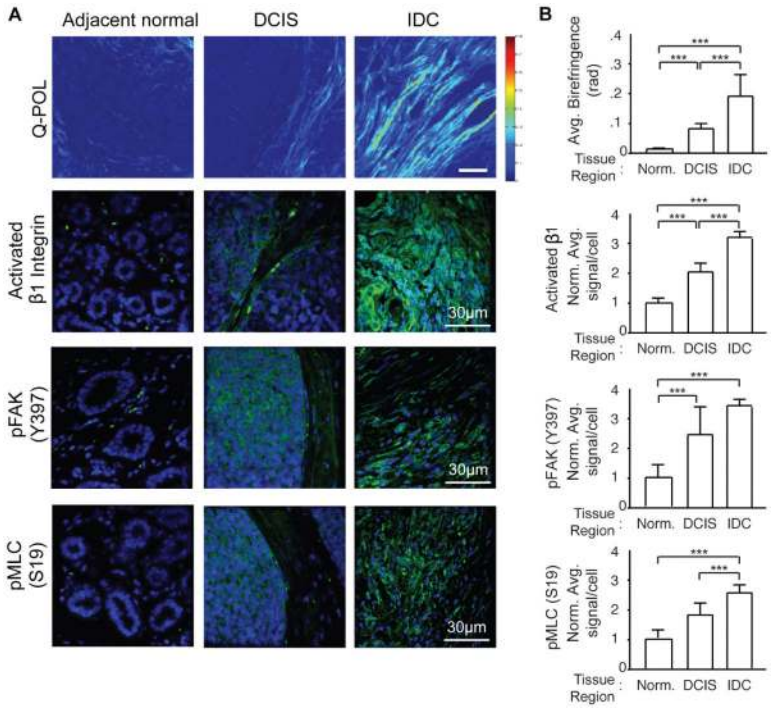

Figure 2. Human tumor progression is accompanied by increased stromal density and enhanced mechanosignaling

(A) Q-POL and immunofluorescence imaging of human tumor samples. Q-POL images shown as a heat map of birefringence reflecting increased stromal density, alignment, and stiffness. Immunofluorescence imaging for mechanosignaling in the tumors includes activated beta 1 integrin, pFAK (Y397), and pMLC (S19). (B) Quantification of Q-POL and immunofluorescence imaging. Immunofluorescence quantified as average signal intensity per cell. Bars represent average of 20 patient samples and error bars represent standard deviation. (*** denotes $P<0.05$)

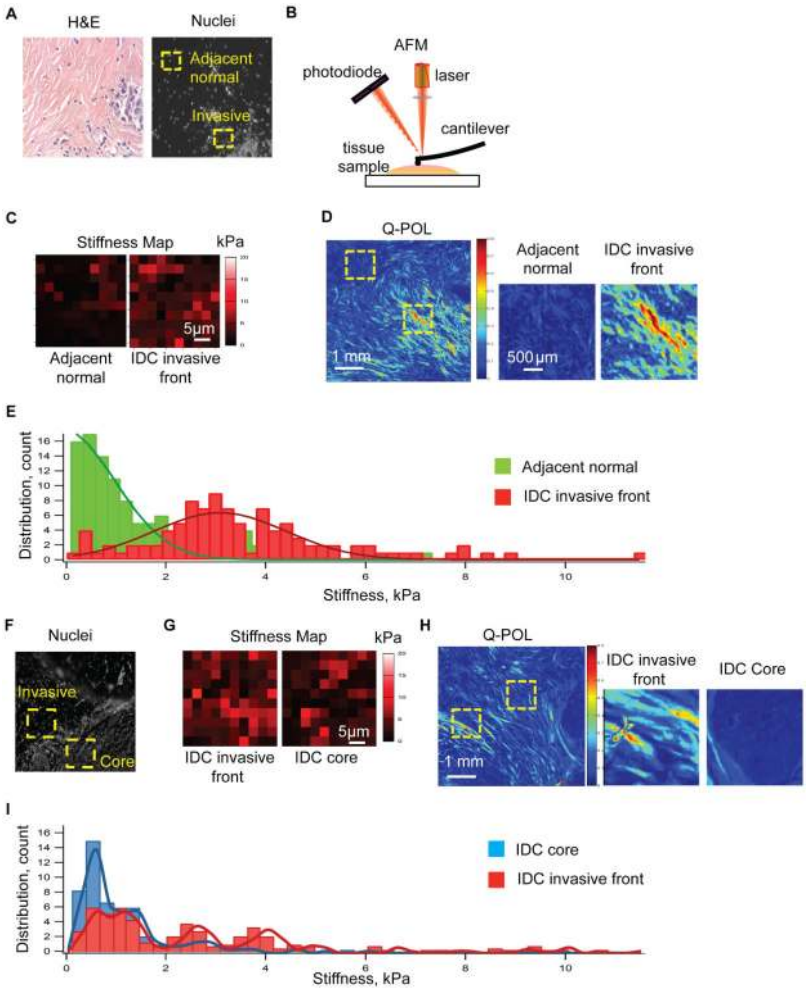

Figure 3. ECM remodeling at the tumor invasive front is correlated with increased ECM stiffness

(A) H&E staining and nuclear immunofluorescence images used to determine regions for atomic force microscopy (AFM) testing comparing tumor invasive front and adjacent healthy tissue. (B) AFM schematic (C) AFM force map result represented as a heat map. (D) Q-POL imaging comparing adjacent normal tissue and tumor invasive front measured via AFM. (E) Histograms of stiffness values from adjacent normal tissue and tumor invasive front. (F) Nuclear immunofluorescence images used to determine regions for atomic force microscopy (AFM) testing comparing tumor invasive front and tumor core. (G) AFM force map result represented as a heat map. (H) Q-POL imaging comparing tumor core and tumor invasive front measured via AFM. (I) Histograms of stiffness values from tumor core and tumor invasive front.

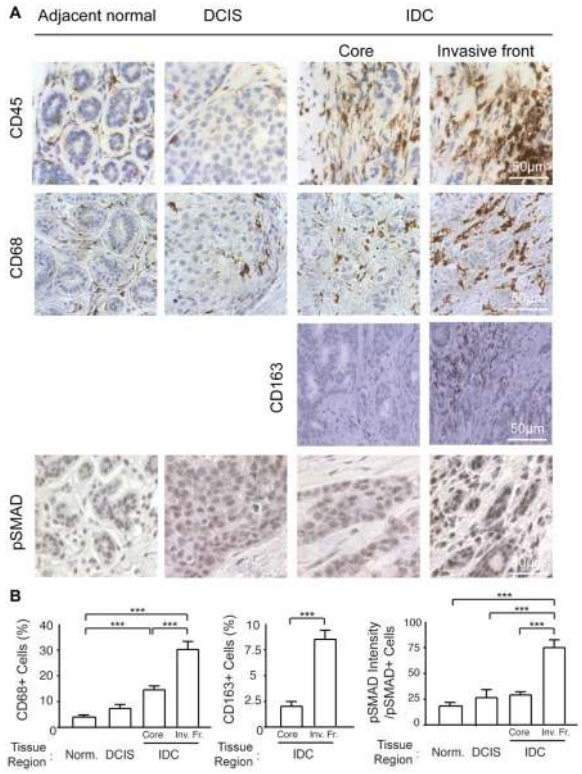

Figure 4. ECM remodeling and stiffening with tumor progression correlates with increased immune infiltrate

(A) Immunohistological staining to assess total immune infiltrate (CD45), macrophage infiltrate (CD68, CD163) and associated tumor cell signaling (pSMAD) comparing healthy, DCIS and IDC tissue. IDC tissue analysis was broken down further comparing the tumor invasive front and the tumor core. (B) Quantification of CD68 and CD163 infiltrate determined as a percentage of CD68+ relative to all cells and quantification of pSMAD signaling assessed as pSMAD staining intensity per pSMAD+ cell. Bars represent average of 20 patient samples and error bars represent standard deviation. (*** denotes P<.05)

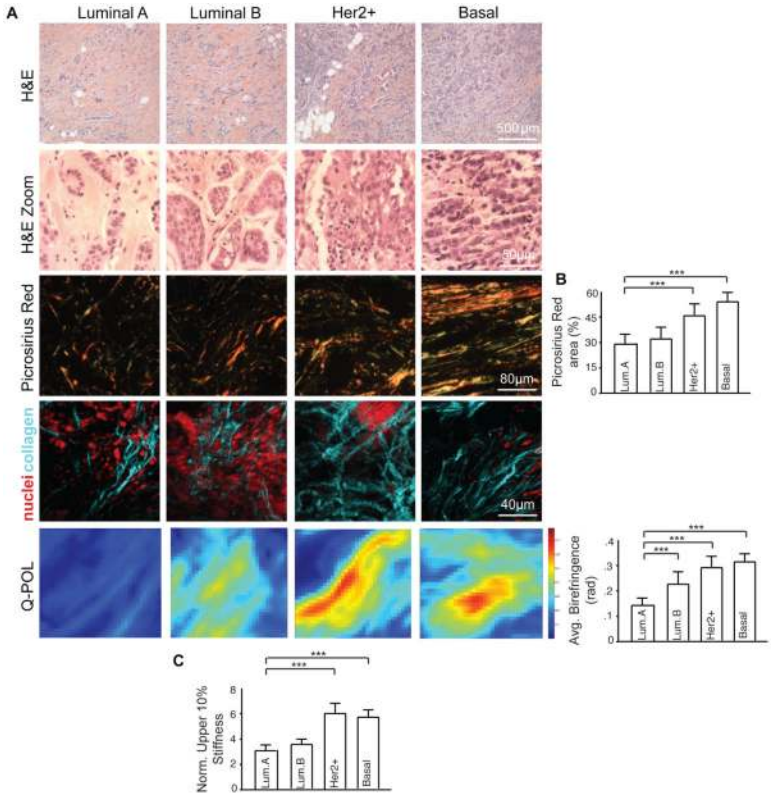

Figure 5. Human breast cancer subtype influences ECM remodeling and mechanics associated with IDC

(A) Immunohistological staining (H&E, picrosirius red and second harmonic generation) and imaging of human tumor samples featuring areas of different subtypes (Luminal A, Luminal B, Her2+ and Basal). (B) Quantification of picrosirius red area and Q-POL imaging as a measure of collagen density, tissue birefringence and mechanics. (C) Quantification of AFM measurements of human tissue samples. The upper 10% of stiffness values are shown and normalized to measurements from prophylaxis tissue serving as a normal control. Bars represent an average of 5 patient samples per subtype and error bars represent standard deviation. (*** denotes $P<0.05$)

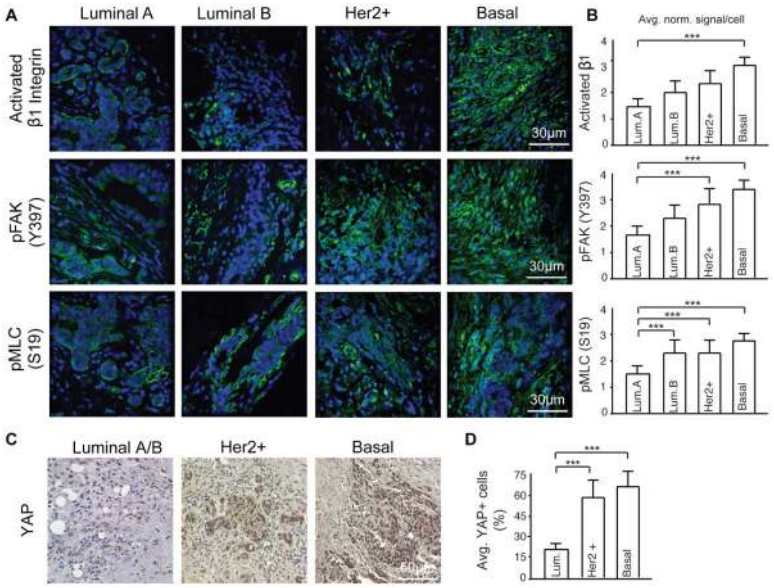

Figure 6. ECM remodeling associated with each subtype influences subsequent mechanosignaling

(A) Immunofluorescence imaging for mechanosignaling in the tumors including activated beta 1 integrin, pFAK (Y397), and pMLC (S19). (B) Quantification of immunofluorescence as average signal intensity per cell. (C) Immunohistological staining for YAP. Luminal A and Luminal B tumors assessed as one group due to lack of differences in YAP intensity. (D) Quantification of YAP staining as average percentage of nuclear YAP+ cells per patient within each subtype. Bars represent an average of 5 patient samples per subtype and error bars represent standard deviation. (*** denotes $P<0.05$)

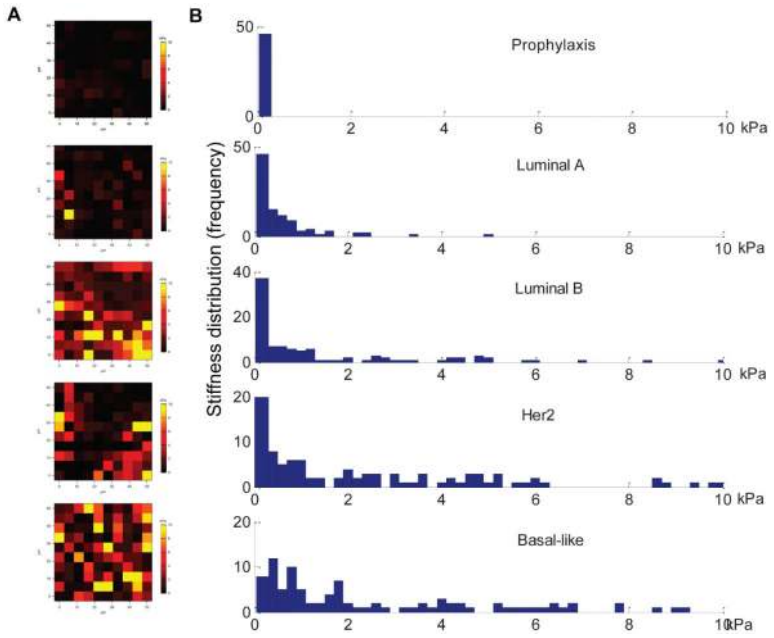

Figure 7. AFM testing of human tissue reveals increased mechanical heterogeneity within the more aggressive subtypes

(A) Atomic force microscopy sample force map result represented as a heat map. (B) Histograms of AFM mechanical measurements for human prophylaxis tissue and human tumor tissue of each subtype. Statistical significance was determined via a Wilcoxon Rank Sum Test, with all subtypes showing statistically significant differences relative to prophylaxis tissue ($p<0.05$).

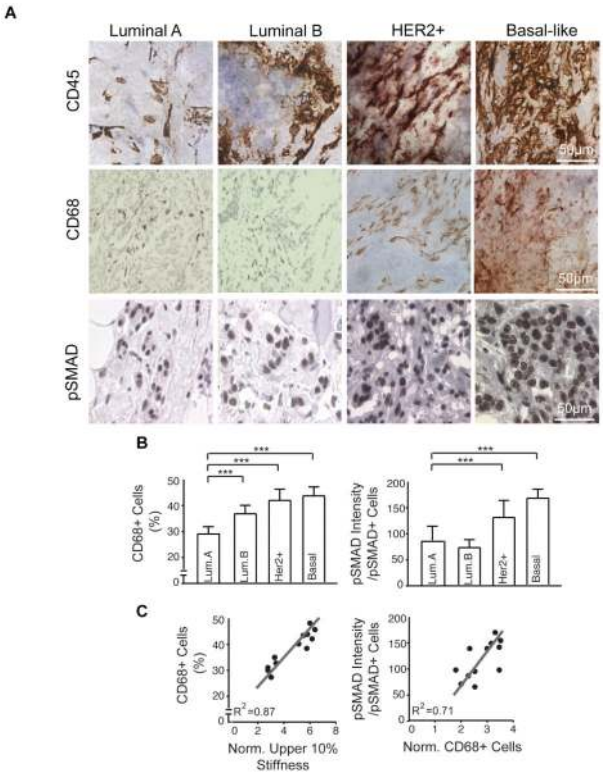

Figure 8. Tumor aggression and increased immune infiltrate correlates with ECM stiffness

(A) Immunohistological staining to assess total immune infiltrate (CD45), macrophage infiltrate (CD68), and associated tumor cell signaling (pSMAD) comparing breast cancer human subtype. IDC tissue analysis was broken down further comparing tumor invasive front and tumor core. (B) Quantification of CD68 infiltrate determined as a percentage of CD68+ relative to all cells and quantification of pSMAD signaling assessed as pSMAD staining intensity per pSMAD+ cell. (C) Correlation curves comparing ECM stiffness and macrophage infiltrate and macrophage infiltrate and pSMAD signaling. Curve fit via linear regression model. Bars represent an average of 5 patient samples per subtype and error bars represent standard deviation. (*** denotes P<0.05)